NANO LETTERS

Letter

pubs.acs.org/NanoLett

Strengthening in Graphene Oxide Nanosheets: Bridging the Gap between Interplanar and Intraplanar Fracture

Changhong Cao,[†,⊥] Matthew Daly,[‡,⊥] Brandon Chen,[†] Jane Y. Howe,[‡,§] Chandra Veer Singh,[*,‡] Tobin Filleter,[*,†] and Yu Sun[*,†]

[†]Department of Mechanical and Industrial Engineering, University of Toronto, Toronto, Ontario M5S 3G8, Canada

[‡]Department of Materials Science and Engineering, University of Toronto, Toronto, Ontario M5S 3E4, Canada

[§]Hitachi High-Technologies Canada, Inc., 89 Galaxy Blvd, Suite 14, Toronto, Ontario M9W 6A4, Canada

Supporting Information

ABSTRACT: Graphene oxide (GO) is a layered material comprised of hierarchical features which possess vastly differing characteristic dimensions. GO nanosheets represent the critical hierarchical structure which bridges the length-scale of monolayer and bulk material architectures. In this study, the strength and fracture behavior of GO nanosheets were examined. Under uniaxial loading, the tensile strength of the nanosheets was measured to be as high as 12 ± 4 GPa, which approaches the intrinsic strength of monolayer GO and is orders of magnitude higher than that of bulk GO materials. During mechanical failure, brittle fracture was observed in a highly localized region through the cross-section of the nanosheets without interlayer pull-out. This transition in the failure behavior from interplanar fracture, common for bulk GO, to intraplanar fracture, which dominates failure in monolayer GO, is responsible for the high strength measured in the nanosheets. Molecular dynamics simulations indicate that the elastic release from the propagation of intraplanar cracks initiates global fracture due to interlayer load transmission through hydrogen bond networks within the gallery space of the GO nanosheets. Furthermore, the GO nanosheet strength and stiffness were found to be strongly correlated to the effective volume and thickness of the samples, respectively. These findings help to bridge the understanding of the mechanical behavior of hierarchical GO materials and will ultimately guide the application of this intermediate scale material.

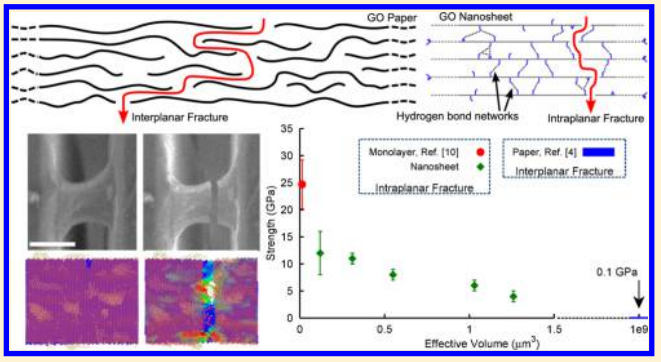

KEYWORDS: *Graphene oxide, nanomechanical testing, molecular dynamics, mechanical properties, fracture*

Graphene oxide (GO) nanosheets, with thicknesses ranging from 10 to 100 nm,[1,2] are a hierarchical structural unit whose characteristic dimension lies between monolayer GO films (0.6−1.2 nm)[3] and GO papers (≳1 μm).[4−6] Formed from a stacking of monolayer GO flakes, GO nanosheets can in-turn be layered to create bulk GO structures (see Figure 1). In this regard, GO nanosheets represent an important intermediate structural unit within the hierarchy of GO materials. GO nanosheets have been used in composites for structural reinforcement[1] and have also been implemented for humidity sensing.[2] Additionally, GO nanosheets possess excellent conductivity and optical transmittance after reduction and can be implemented in flexible electronics,[7] supercapacitors,[8] and transparent conductive films.[9] Given that many of these applications of GO nanosheets require optimal mechanical properties, such as high strength and fracture toughness, an understanding of the length-scale dependence of mechanical behavior in GO materials is of great importance toward tailoring material architecture to meet performance requirements. Although GO nanosheets represent a key structural unit, so far the strength and fracture behavior of GO nanosheets have not been investigated.

Existing studies have reported the strength of monolayer GO and bulk GO paper to be 24.7 GPa[10] and ∼100 MPa,[4,6] respectively, suggesting a significant impact of length scale on mechanical properties. This orders of magnitude discrepancy in strength originates from the distinct failure mechanisms operative at each length scale. Specifically, monolayer GO has been shown to achieve intrinsic strength through cleavage of atomic bonds along a path that connects functionalized carbon atoms in the basal plane,[10] whereas GO paper typically fails by an interplanar process of delamination and shear deformation along microdefects.[6] For intermediate length-scale materials, such as GO nanosheets which exhibit significantly different structural characteristics, it is expected that the strength and failure mode would deviate significantly from GO paper. In a

Received: June 2, 2015
Revised: August 17, 2015
Published: September 4, 2015

DOI: 10.1021/acs.nanolett.5b02173
Nano Lett. 2015, 15, 6528−6534

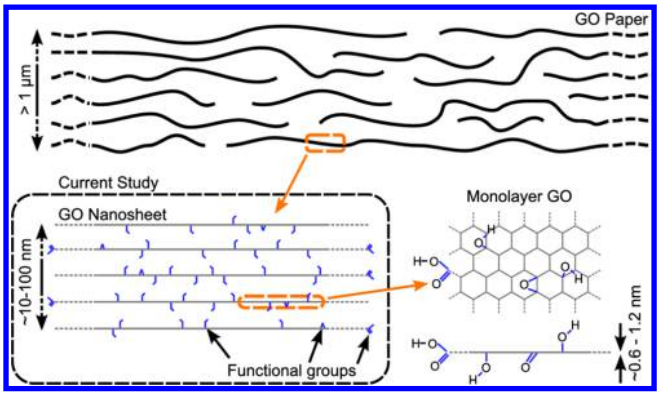

Figure 1. Schematic of the hierarchical units forming the basis of GO materials. GO nanosheets are comprised of a closely packed layering of monolayer GO flakes. GO papers are formed from a heterogeneous stacking of GO nanosheets. Due to the nonuniform layering of GO nanosheets, the gallery space in GO papers is populated by a distribution of voids. The functional groups are specified as per the Lerf–Klinowski model.[22]

recent study, Wang et al.[11] examined the mechanical properties of GO flakes by adhering the tip of an atomic force microscopy (AFM) cantilever to GO deposited on carbon fiber. However, the intrinsic strength and fracture behavior of GO nanosheets remains unknown due to (1) the heterogeneous loading induced in the GO monolayer which was directly bonded to the AFM cantilever; (2) the prevalence of individual layer rupture and pull-out directly surrounding the bonded region.

A major challenge in the investigation of mechanical properties of ultrathin structures (e.g., GO nanosheets) is the lack of techniques for mechanical testing and transfer of these films. Traditional approaches such as macro-scale tensile testing (used for testing bulk GO papers[6,12]) are not suitable due to dimensional limitations of the instrumentation. Conversely, localized nanomechanical methods such as nanoindentation or AFM deflection testing, which is a common tool for measuring the strength of monolayer GO,[10] are not suitable in the case of GO nanosheets. Specifically, in GO nanosheets the influence of unknown interfacial shear interactions between layers is required for strength analysis. Furthermore, these nanomechanical testing platforms are capable of probing only very localized properties in thin films. To overcome these limitations, in situ scanning electron microscope (SEM) and transmission electron microscope (TEM) tensile and compressive testing platforms have been developed to manipulate nanostructures and measure their physical properties directly. For example, in situ experiments have been previously conducted to measure the mechanical properties of 1D nanostructures such as nanotubes[13,14] and nanowires[13,15] using microelectromechanical systems (MEMS). However, due to unavoidable buckling and folding of thin films during pickup, nanomanipulation techniques implemented for transferring 1D nanostructures onto MEMS devices are not suitable for the transfer of GO nanosheets. In a recent study, Zhang et al.[16] measured the fracture toughness of graphene using a nanoindentor-actuated tensile MEMS device. However, this technique is not suitable for solution-based materials, such as the GO nanosheets studied herein, which cannot be placed via dry-transfer methods. Additionally, such a system is externally actuated by the motion of the nanoindentor head which may cause slippage at contact points to the actuation shuttles and misalignment of the shuttles with the nanoindentor axis.

In the present study, the strength and fracture behavior of GO nanosheets was investigated using a combined experimental and computational approach. In order to circumvent existing issues with transfer and testing of ultrathin films, the tensile stress–strain response of GO nanosheets was measured under electron microscopy imaging using a customized monolithic Si MEMS device with two symmetrical integrated thermal actuators. Digital image processing was used to correlate electron microscopy images and to determine the mechanical response of the GO nanosheets. During mechanical testing, highly localized fracture behavior was observed in the GO nanosheets. Molecular dynamics (MD) simulations were utilized to investigate the atomistic origins of the fracture process. Results indicate that GO nanosheets possess strengths approaching monolayer values. The current investigation is the first report of strength assessment in GO nanosheets, serving to populate a previously unexplored region of material-property space. The physical phenomena studied in this intermediate hierarchical structure highlight a transition in failure behavior, from the interplanar dominated fracture observed in bulk GO papers to the intraplanar bond-cleavage mechanism responsible for intrinsic strength in monolayer GO. This intermediate length-scale thus permits access to impressive strengthening characteristics, without the restriction to monolayer GO preparations, which are difficult to synthesize and are limited in scalability.

An SEM image of the Si MEMS device used for uniaxial tensile tests is presented in Figure 2a, and a schematic of the in situ experimental setup is provided in the inset. In contrast to the nanoindentor-actuated device used for characterizing the fracture toughness of graphene, by integrating the thermally driven microactuators directly into the device, the MEMS tensile tester enables a streamlined experimental characterization route. This permits the mechanical characterization of the film-based structure on a single chip and without assistance from external devices, which minimizes instrumental errors. As shown in Figure 2a, the Si MEMS device contains two symmetrical thermal actuators coupled with heat sink beams on either side of a gap (gap varies from ~1.3 to 2.2 μm) over which the specimen is placed. The two actuation shuttles are on the same plane to avoid any out-of-plane motion during tensile loading. When a voltage is applied, the two actuation shuttles move in opposite directions. Actuation displacements and reaction forces were experimentally calibrated[17] (see the Supporting Information) prior to GO testing. In order to avoid intricate manipulation of GO samples, a simple GO nanosheet preparation process was developed. Large GO flakes, with lateral dimensions exceeding 1 μm (smaller flakes were filtered out during the two-step centrifuge process[10,18] (see the Supporting Information) were drop-cast over the gap between the two actuation shuttles using a custom-built micropipetting system.[19] Prior to mechanical testing, the GO nanosheets were dried for 24 h in air and soft baked at 100 °C for 1 h. After this process, the GO nanosheets were found to be well-adhered to the Si MEMS device. A cross-sectional view of GO nanosheets drop-cast on a Si/SiO_2 wafer (see the Supporting Information) reveals a homogeneous structure and an absence of the obvious large voids or interlayer delamination, which is in direct contrast to the relatively porous cross-section of GO papers.[6,12] GO nanosheets with varying widths, ranging from ~1–9 μm, lengths between 1.3 to 3.9 μm, and thicknesses (between 24 and 75 nm) were studied. The geometrical characteristics of eight different GO nanosheets for which tensile testing was

DOI: 10.1021/acs.nanolett.5b02173
Nano Lett. 2015, 15, 6528–6534

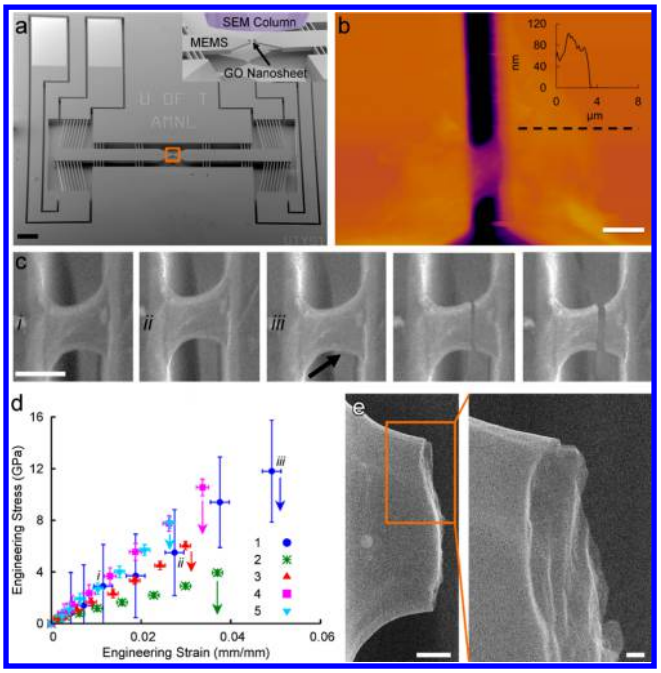

Figure 2. (a) SEM image of the integrated MEMS device, which possesses two symmetrical thermal actuators (scale bar: 200 μm). The orange box indicates the placement region for GO nanosheets. Inset: high magnification schematic showing the in situ experimental setup with a GO nanosheet suspended over the MEMS device inside the SEM (b) AFM tapping mode topography image of a GO nanosheet (scale bar: 2 μm) (not used for lateral dimension measurement). Inset: height profile of the dashed line. A height of approximately 75 nm was measured. (c) SEM images of a suspended GO nanosheet during tensile testing at increasing actuations. The black arrow indicates the site of fracture initiation (scale bar: 1 μm). Fracture is observed to progress in a highly localized region through the entire thickness of the GO nanosheet. (d) Stress–strain data from five tensile tests. The italicized callouts refer to the loading-state of the corresponding SEM images in c. (e) Post-mortem STEM images of a different GO nanosheet after failure (scale bars: left: 500 nm; right: 100 nm). The fracture of separate GO flakes is visible in the image. All SEM and STEM images use the secondary electron signal to form image contrast. The higher magnification STEM image in e has been tilted to better show the GO nanosheet cleavage morphology.

performed are provided in the Supporting Information. The thickness of each of these GO nanosheets was measured using tapping mode AFM topography imaging on the film edges (see Figure 2b) and was validated by electron energy loss spectroscopy (EELS) thickness mapping[20] (see the Supporting Information). It should be noted that the lateral dimensions (i.e., length and width) of the GO nanosheets cannot be accurately measured by AFM imaging due to AFM tip access restrictions within large step height changes, which can artificially inflate values. Therefore, all lateral dimensions were measured directly by electron microscopy imaging.

Figure 2c shows a suspended GO nanosheet at varying stages of uniaxial tensile loading. The analysis methodology for the determination of nanosheet stress and strains as well as the associated error analysis is provided in the Supporting Information. Elastic loading and unloading of the sample up to a strain of 3% was conducted before the sample was stretched to failure (~5%) in order to identify potential slippage between the GO nanosheet and actuation shuttles and to measure the Young's modulus. Any hysteresis observed was well within the measurement error in the loading/unloading stress–strain data and there is no obvious wrinkling due to tension from electron microscopy images, confirming the well-fixed boundaries on the edge of the GO nanosheet as well as the good adhesion to the Si MEMS device (see the Supporting Information). The Young's modulus was measured by linear fitting of loading/unloading stress–strain curves and was measured with standard error to be 204 ± 7 GPa, which approaches the value of monolayer GO (207.6 to 384 GPa).[10,21] Tensile tests to measure strength were performed on five GO nanosheet samples (Samples 1– 5), and the resultant stress–strain results are plotted in Figure 2d. Stress and strain are reported in engineering terms. The italicized callouts in the figure indicate the relevant loading in the corresponding SEM images in Figure 2c. Upon reaching the maximum tensile stress, all GO layers were observed to undergo brittle failure via fracture through the entire width of the cross-section and without any significant pull-out behavior. In order to confirm this fracture behavior for the GO nanosheets and identify features of the fracture surface with high resolution, scanning transmission electron microscope (STEM) images were captured from an additional GO nanosheet (Sample 6) tested in situ under the same tensile experiment configuration. As shown in Figure 2e, failure occurred along a uniform cleavage plane through all the layers without any significant interlayer shearing or pull-out. Flake edges are visible in the higher magnification image, indicating that mechanical failure occurred by intraplanar fracture of individual layers within a highly localized region. There does appear to be some degree of crack front separation near the upper edge of the tensile specimen. However, the distance between the flake edges to the fracture plane was measured to be approximately 200 nm, which is smaller than the lateral dimension of average GO flake size (1 μm and above, see the Supporting Information). This further confirmed the lack of significant GO layer pull-out from the nanosheet during tension. This morphology is therefore more likely caused by crack-branching along intraplanar defects during fracture. Furthermore, the orientation of the crack when considered across the entire width of the GO nanosheet was found to be nearly perpendicular to the tensile direction, though zigzag patterns were present in localized regions of specific layers, which could be due to the presence of intraplanar defects. This behavior is also confirmed by two additional tensile straining experiments performed on GO nanosheets with large pre-existing cracks (Samples 7 and 8, see the Supporting Information). The fracture angle was found to be approximately 90° to the loading direction in all eight samples (see the Supporting Information). For the experimental sample with the image sequence shown in Figure 2c, the tensile strength was measured to be 12 ± 4 GPa at a strain of 5% ± 0.2%. Similar experiments to measure strength were performed on the other four GO nanosheets samples. Taken together, the five GO nanosheets loaded to failure exhibited strengths ranging between 4–12 GPa with little plastic behavior observed prior to fracture. A summary of the tensile strength and Young's moduli measurements for Samples 1–5 is provided in Table 1.

SEM imaging of the GO nanosheet cross-section (see the Supporting Information) revealed that adjacent individual GO layers are well-stacked as compared to GO papers, which are known to possess large voids between adjacent sheets[6,12] and exhibit interlayer delamination during failure. Furthermore, the GO nanosheets appear to be continuous across the gauge length in tensile testing (Figure 2c). The typical area of

DOI: 10.1021/acs.nanolett.5b02173
Nano Lett. 2015, 15, 6528–6534

Table 1. Structural and Mechanical Properties of the Tested GO Nanosheets

sample no.	sheet thickness (nm)	effective volume (μm^3)	Young's modulus (GPa)	tensile strength (GPa)
1	75 ± 13	0.12 ± 0.02	204 ± 7	12 ± 4
2	70 ± 11	1.26 ± 0.20	103 ± 5	4 ± 1
3	65 ± 9	1.03 ± 0.14	182 ± 3	6 ± 1
4	24 ± 4	0.31 ± 0.05	291 ± 5	11 ± 1
5	34 ± 14	0.55 ± 0.23	266 ± 5	8 ± 1

monolayer GO flakes synthesized by a similar method is greater than 100 μm^2.[18] Flakes with smaller lateral dimensions were filtered out during sample preparation. Therefore, a relatively homogeneous suspended structure is expected. In comparison to the reported failure mechanisms in GO papers, the uniform stacking of GO nanosheets was found to contribute to the observed brittle intraplanar fracture, which is similar to the dominant failure mechanism in monolayer GO.[10] The fracture is therefore expected to initiate from a critical structural flaw, following a weakest-link failure behavior. Indeed, according to SEM images (see black arrow in Figure 2c), the fracture was observed to initiate from an edge crack. It should be noted that the GO nanosheets did not exhibit a specific preference for edge-dominated fracture initiation; rather, failure was expected to proceed from a path formed by the presence of critical flaws, both internal to the structure and residing at sample edges. Furthermore, given the nature of drop-casting, it is likely that fracture initiated from a critical flaw confined to a small number of layers or possibly even a single layer in the cross-section of the GO nanosheet. Continued loading caused fracture along a cleavage plane nearly perpendicular to the tensile loading direction (see the Supporting Information), with crack propagation confined to trans-layer cracking in a localized region (Figure 2c). However, the explicit mechanism of crack propagation is not directly evident from imaging. During failure, the edge crack may have propagated into adjacent layers of the GO nanosheet to create the observed trans-layer fracture morphology.

In order to understand the atomistic origins of the observed intraplanar trans-layer fracture mechanism, molecular dynamics (MD) simulations were performed. The Lerf–Klinowski model[22] was used as a blueprint to construct GO nanosheets. Previous X-ray photoelectron spectroscopy (XPS) measurements of the GO precursor material used in drop-casting were considered to define the specific functional composition of the GO nanosheets in MD simulations.[23] Guided by the XPS data, GO nanosheet free-edges were terminated with carboxyl functional groups, and given their relatively high count rate from XPS, the GO nanosheets used in our MD studies were terminated up to near complete saturation. Additionally, XPS measurements indicated a 22% functionalization of hydroxyl and/or epoxide groups in the basal plane and an oxygen-to-carbon (O/C) ratio of approximately 1:4. Given the difficulty in differentiating epoxide and hydroxyl chemical states due to their similar binding energies, two different GO nanosheet structures were created for MD simulations, corresponding to the extremes of functionalized structures. In the first structure, a 22% hydroxyl functionalization was assumed (Figure 3a), and in the second structure, a 22% epoxide functionalization was assumed (see the Supporting Information).

In order to elucidate trans-layer crack propagation in the GO nanosheet, an elliptical edge crack was introduced into a single

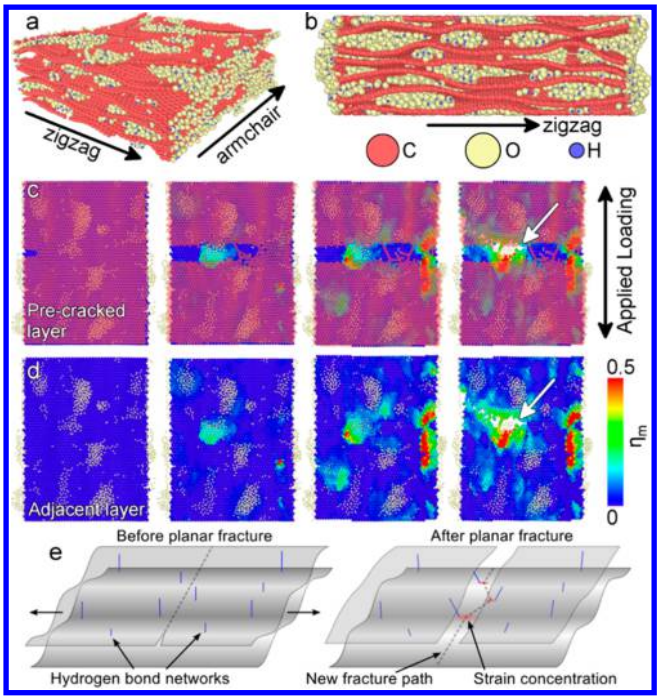

Figure 3. Structure of the hydroxyl functionalized GO nanosheets in (a) perspective and (b) cross-sectional views. Periodic boundary conditions are preserved through the cross-section and along the armchair direction. (c, d) Fracture propagation in the precracked layer for an edge crack of dimension $a = 4a_o$, where a is the half-length of the edge flaw and a_o is the crack quantum. The arrows indicate the site of crack initiation in the adjacent layer. The precracked layer is made translucent in c and is removed in d in order to provide a correlated perspective for crack initiation events. The atomic strain map in the adjacent basal plane is illustrated along with the intercalated functional group agglomerations. The size of oxygen atoms has been reduced, and hydrogen atoms have been removed for clarity purposes. Lagrangian strains are all referenced to the configuration just prior to fracture in the precracked layer. (e) The proposed mechanism for localized translayer fracture propagation. The application of uniaxial tension confines functional group agglomerates into the basins of long-range corrugations in the basal plane. The elastic release from fracture in the precracked layer transmits strain energy through nearby agglomerates via hydrogen bond networks into the adjacent basal plane, creating a strain concentration which serves as a site for subsequent crack initiation and a critical path for continued fracture.

layer of the basal plane prior to uniaxial loading. Although the critical flaw could possess any range of morphologies, the use of the elliptical edge crack is preferred in order to implement existing analytical approaches for brittle failure, such as Griffith theory.[24] The half-length of the edge crack (a) was selected to be an integral multiple of the crack quantum (a_o). Initial precracked lengths were increased in $2a_o$ increments from a_o to $10a_o$, which represented less than 25% of the supercell width. Pre-existing flaws larger than this relative dimension were not observed in the *in situ* experimental studies and were therefore not considered in MD simulations. As per previous MD studies, a_o represents the width of the hexagonal unit cell in the direction perpendicular to loading.[25] During relaxation and equilibration of the MD supercell, functional groups were observed to reorganize and form agglomerated complexes in the gallery space. These agglomerations of functional groups were found to be approximately 1–2 nm in size and effectively partitioned the basal planes into heavily oxidized and graphene-like regions (see the Supporting Information). These

DOI: 10.1021/acs.nanolett.5b02173
Nano Lett. 2015, 15, 6528–6534

observations are consistent with recent first-principles calculations of functional group chemical and kinetic stability in the GO material system[26] as well as high resolution TEM studies which revealed heterogeneous distributions of oxygen into localized regions on monolayer GO.[27] Consequently, these agglomerations caused distortions in the gallery space of GO and created undulations in the carbon basal planes (Figures 3a and b). The peaks and valleys of these undulations were found to range between 0.4 and 0.7 nm in amplitude (see the Supporting Information), which is consistent with AFM roughness measurements of GO films with an O/C ratio of 1:5.[28] Under the presence of uniaxial tension, these undulations were observed to align to the loading direction and form long-range corrugations which were directed perpendicular to the applied loading. Interestingly, these corrugations served as basins for the collection of kinetically active functional groups which created regions of both local excess and dearth of functional agglomerates (see the Supporting Information). The concentration of functional groups into these strain-induced corrugations created hydrogen bond networks that interconnected adjacent layers in the GO nanosheets. The formation of hydrogen bond networks between layers in GO structures is consistent with previous MD studies of GO structures.[29,30]

Under continued loading, mechanical fracture of the GO nanosheet was observed to initiate from the crack tip and propagate through the basal plane in all MD simulations, conforming to a Mode I fracture behavior. Additional MD simulations of GO nanosheets with precrack lengths of $2a_o$ and $8a_o$ are provided in the Supporting Information. In each precracked sample, a stress concentration was observed to form in a narrow region surrounding the edge crack, suggesting an absence of a plastic zone and leading to the initiation of a highly brittle fracture mechanism (see the Supporting Information). The stress intensity factor was found to increase monotonically with crack length and was calculated to be in the range of 2.3−4.9 for the GO nanosheets examined in this study. Figure 3c illustrates the fracture path through the precracked layer ($a = 4a_o$) as well as the atomic strain map in the basal plane of the adjacent GO layer. Atomic strain is defined here in the Lagrangian formulation as the local strain hydrostatic invariant (η_m) which may be derived directly from the definition of the local deformation gradient.[31] As the crack propagated past a cluster of functional groups in a confined corrugated region, a localized strain concentration was observed to develop (Figure 3d). Just prior to fracture, relative hydrostatic strains of approximately 0.5 above the far-field loadings were measured at the crack initiation site in the adjacent layer. From a mechanistic perspective, the strain energy released during crack propagation in the precracked layer was transmitted through the nearby network of hydrogen bonds in the functional group agglomerations to a localized area in the adjacent carbon layer (Figure 3e). In this regard, the functional group agglomerates served to bind the fractured layer with the remaining GO nanosheet. Due to the geometric confinement imposed by the strain-induced corrugations in the carbon basal planes, the movement of functional group agglomerates was restricted. This mobility-constraint limited the amount of deformation accommodation to cracking. Continued loading of the GO nanosheet therefore caused further stretching in the hydrogen bond network and subsequently increased the magnitude of the strain concentration until crack initiation in the adjacent layer occurred. Using Griffith theory (see the Supporting Information), the elastic energy release rate in GO was calculated to be approximately 13.1 J/m^2, which approaches the experimental value for graphene (15.9 J/m^2[16]) and is notably high for a brittle material (see the Supporting Information). In comparison to another typical brittle material, the elastic energy release rate of soda-lime-silica glass is reported to be approximately 5 J/m^2.[32] The transmission of this relatively large elastic energy through functional group networks is responsible for the development of the strain concentrations observed in MD simulations.

These tensile simulations were repeated for epoxide functionalized samples, and in contrast to hydroxyl functionalized GO nanosheets, correlated fracture events were not observed in adjacent layers (see the Supporting Information). Owing to the absence of a hydrogen bond network in this GO nanosheet, the fracture propagation mechanism shown in Figure 3e was not observed. Indeed, the epoxide functionalized samples were prone to formation of planar defects during loading which encouraged uncorrelated fracture events between adjacent layers in the GO nanosheet. As a result, fracture did not necessarily progress along a path perpendicular to the applied loading in contrast to that observed for experimental GO nanosheets. It should be noted that a combination of both hydroxyl and epoxide functional groups are expected in the experimental GO nanosheets. Therefore, these MD simulations represent the bounding behavior of potential fracture mechanisms. According to recent first-principles calculations, the hydroxyl functional groups are kinetically stable, and the reduction of epoxide groups is favored.[33] In this regard and considering the observed experimental fracture mechanism, the presence of functional agglomerations permits the transmission of elastic energy through hydrogen bond networks and is believed to underpin the dominant failure process in GO nanosheets.

Relative to bulk GO paper, the strengths measured in this study for GO nanosheets are found to be orders of magnitude higher, approaching monolayer GO values. The observed differences in strength can be explained by the fundamental differences in material architecture at each length-scale. While GO nanosheets are formed by a closely packed layering of monolayer GO flakes, bulk GO papers are comprised of a heterogeneous stacking of GO nanosheets, which possess interlayer voids and large defects.[6,12] As a result of this discontinuous and disrupted stacking of hierarchical units, bulk GO samples undergo an interplanar fracture mechanism during tensile loading, whereby failure occurs along a critical path that follows interlayer defects (Figure 4a).[6] Conversely, structurally homogeneous GO nanosheets are observed to fail at very high loadings by a highly localized intraplanar fracture mechanism. This failure behavior is made possible by a hydrogen bond network which serves to interconnect GO monolayers into a well-stacked architecture. Failure then initiates from a critical in-plane flaw and propagates through a layer of the nanosheet. The elastic energy release from this fracture event is transmitted via the hydrogen bond network to adjacent layers, initiating subsequent fracture events within a highly localized region in the GO nanosheet (Figures 4b, c).

In a pristine condition with perfect bonding between layers, GO nanosheets should possess a near-intrinsic strength (i.e., the strength of monolayer GO) under uniaxial tensile loading. However, due to the presence of planar defects and the new possible failure pathway imposed by the layered structure, the strength of the GO nanosheets tested experimentally in the current study is lower than intrinsic values at comparable

DOI: 10.1021/acs.nanolett.5b02173
Nano Lett. 2015, 15, 6528−6534

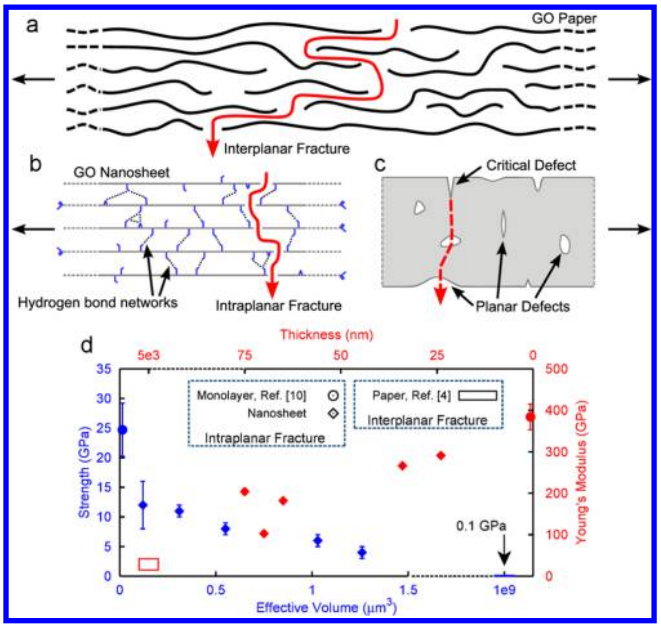

Figure 4. (a) Interplanar fracture mechanism that is dominant in bulk GO papers.[4] Under uniaxial loading, fracture progresses along a critical path formed by voids and defects in the gallery space between GO nanosheets. (b) The localized intraplanar fracture mechanism observed in failure of GO nanosheets (cross-section view). (c) Fracture initiates along a critical path within a monolayer GO flake and then propagates into adjacent layers through transmission of elastic energy via hydrogen bond networks (planar view).[10] (d) The influence of sample volume on measured strength in GO nanosheets and the relationship between sample thickness and Young's modulus. The comparative strengths and Young's moduli of monolayer GO and GO papers are provided as a benchmark.

sample chemistries.[10] Indeed, the GO nanosheets also exhibit variations in strength which are strongly correlated to the effective volume (Table 1). The influence of effective loading volume is considered against measured strength in Figure 4d. The strengths for monolayer GO (AFM testing)[10] and GO papers (tensile testing)[4] are plotted for comparison. In the case of monolayer GO, the effective volume is assumed to be the amount of material directly under the AFM cantilever, using the reported tip dimensions (assumed monolayer thickness of 0.7 nm multiplied by the contact area between the AFM tip and the GO film).[10] As shown in the figure, there is an inverse relation between effective volume and sample strength. According to Weibull statitistics,[34] larger GO nanosheet volumes are more likely to possess larger planar defects which lower the threshold to mechanical failure and adversely impact strength. Furthermore, it was observed that the Young's modulus can also be inversely correlated to sample thickness (Figure 4d). In this regard, the stiffness of the GO nanosheets was found to approach that of monolayer GO (384 GPa)[10] and was much higher than reported values for GO papers (15−42 GPa).[4] Taken together, trends observed in both strength and stiffness provide strong evidence of the scaling effects on the mechanical properties of GO materials. It is likely that the effects of GO roughness, interlayer voids, and functional group clusters inhibit a linear scaling of layer stacking with film thickness, leading to a decrease in effective stiffness at larger sample dimensions. Further study is required to confirm this geometric effect.

Relative to GO papers, the results of the current study show a significant increase in strength and serve to populate a previously unexplored region of material−property space in GO materials. The physical phenomena underpinning mechanical stability in this intermediate hierarchical structure highlight an important transition in failure behavior, from the interplanar dominated fracture observed in bulk GO papers toward the intraplanar bond-cleavage mechanism responsible for the high intrinsic strength in monolayer GO. These findings help to bridge the understanding of the mechanical behavior of hierarchical GO materials and will ultimately guide both the application of this intermediate scale material, as well as improvements in the synthesis of macroscopic GO papers and films.

■ ASSOCIATED CONTENT

Supporting Information

The Supporting Information is available free of charge on the ACS Publications website at DOI: 10.1021/acs.nanolett.5b02173.

Experimental section, force calibration, error analysis, geometrical measurements of GO nanosheets, AFM imaging of lateral GO flakes and cross-sectional imaging of the GO nanosheet, electron energy loss spectroscopy (EELS) thickness map of GO, GO samples with pre-existing crack, additional experimental data, tensile simulation of defect-free GO nanosheets, undulations and strain-induced corrugations in GO nanosheets, fracture of GO nanosheets with an edge crack, elastic energy release rate in GO nanosheets, fracture in epoxide functionalized GO nanosheets (PDF)

■ AUTHOR INFORMATION

Corresponding Authors

*E-mail: sun@mie.utoronto.ca.
*E-mail: filleter@mie.utoronto.ca.
*E-mail: chandraveer.singh@utoronto.ca.

Author Contributions

⊥C.C. and M.D. contributed equally to this work.

C.V.S., T.F., and Y.S. conceived the idea and designed the project. T.F. and Y.S. directed C.C. to conduct experiments and analyze the data. C.V.S. directed M.D. to perform the molecular dynamics simulations. Y.S. directed B.K.C. and C.C. to carry out the MEMS design and the in situ experiment setup. C.C. and M.D. both contributed to electron imaging and focused ion beam milling efforts. C.C. and M.D. cowrote the paper under guidance from C.V.S., T.F., and Y.S. All authors discussed the results.

Notes

The authors declare no competing financial interest.

■ ACKNOWLEDGMENTS

The authors acknowledge funding by the Natural Sciences and Engineering Research Council of Canada (NSERC) through Discovery Grants to C.V.S., T.F., and Y.S., a Strategic Project Grant to Y.S., and a Postgraduate Scholarship (PGS) to M.D., and funding from the Canada Foundation for Innovation (CFI). Y.S. also acknowledges financial support from the Canada Research Chairs Program. MEMS fabrication technical support was provided by CMC Microsystem. The authors thank Dr. Patrick Woo, Dr. Stas Dogel, and Charles Soong (Hitachi High Tech, Canada), Dr. Doug Perovic, Sal Boccia,

DOI: 10.1021/acs.nanolett.5b02173
Nano Lett. 2015, 15, 6528−6534

Jun Wen, and Jun Liu (University of Toronto) for technical assistance and discussion. The authors would also like to thank Toronto Nanofabrication Center for fabrication support as well as the Ontario Center for Characterization of Advanced Materials (OCCAM) for electron microscopy and focused ion beam milling support. Molecular dynamics simulations were performed on the Guillimin High Performance Computing (HPC) cluster under the administration of Calculquebec and Compute Canada.

REFERENCES

(1) Cai, D.; Song, M. A simple route to enhance the interface between graphite oxide nanoplatelets and a semi-crystalline polymer for stress transfer. *Nanotechnology* **2009**, *20* (31), 315708.
(2) Borini, S.; White, R.; Wei, D.; Astley, M.; Haque, S.; Spigone, E.; Harris, N.; Kivioja, J.; Ryhänen, T. Ultrafast Graphene Oxide Humidity Sensors. *ACS Nano* **2013**, *7* (12), 11166−11173.
(3) Stankovich, S.; Dikin, D. A.; Piner, R. D.; Kohlhaas, K. A.; Kleinhammes, A.; Jia, Y.; Wu, Y.; Nguyen, S. T.; Ruoff, R. S. Synthesis of graphene-based nanosheets via chemical reduction of exfoliated graphite oxide. *Carbon* **2007**, *45* (7), 1558−1565.
(4) Dikin, D. A.; Stankovich, S.; Zimney, E. J.; Piner, R. D.; Dommett, G. H. B.; Evmenenko, G.; Nguyen, S. T.; Ruoff, R. S. Preparation and characterization of graphene oxide paper. *Nature* **2007**, *448* (7152), 457−460.
(5) Park, S.; Lee, K.-S.; Bozoklu, G.; Cai, W.; Nguyen, S. T.; Ruoff, R. S. Graphene Oxide Papers Modified by Divalent Ions—Enhancing Mechanical Properties via Chemical Cross-Linking. *ACS Nano* **2008**, *2* (3), 572−578.
(6) Gao, Y.; Liu, L.-Q.; Zu, S.-Z.; Peng, K.; Zhou, D.; Han, B.-H.; Zhang, Z. The effect of interlayer adhesion on the mechanical behaviors of macroscopic graphene oxide papers. *ACS Nano* **2011**, *5* (3), 2134−2141.
(7) Wang, J.; Liang, M.; Fang, Y.; Qiu, T.; Zhang, J.; Zhi, L. Rod-Coating: Towards Large-Area Fabrication of Uniform Reduced Graphene Oxide Films for Flexible Touch Screens. *Adv. Mater.* **2012**, *24* (21), 2874−2878.
(8) Kim, M.; Lee, C.; Jang, J. Fabrication of Highly Flexible, Scalable, and High-Performance Supercapacitors Using Polyaniline/Reduced Graphene Oxide Film with Enhanced Electrical Conductivity and Crystallinity. *Adv. Funct. Mater.* **2014**, *24* (17), 2489−2499.
(9) De, S.; King, P. J.; Lotya, M.; O'Neill, A.; Doherty, E. M.; Hernandez, Y.; Duesberg, G. S.; Coleman, J. N. Flexible, Transparent, Conducting Films of Randomly Stacked Graphene from Surfactant-Stabilized, Oxide-Free Graphene Dispersions. *Small* **2010**, *6* (3), 458−464.
(10) Cao, C.; Daly, M.; Singh, C. V.; Sun, Y.; Filleter, T. High strength measurement of monolayer graphene oxide. *Carbon* **2015**, *81* (0), 497−504.
(11) Wang, C.; Peng, Q.; Wu, J.; He, X.; Tong, L.; Luo, Q.; Li, J.; Moody, S.; Liu, H.; Wang, R.; Du, S.; Li, Y. Mechanical characteristics of individual multi-layer graphene-oxide sheets under direct tensile loading. *Carbon* **2014**, *80* (0), 279−289.
(12) Wang, C.; Frogley, M. D.; Cinque, G.; Liu, L.-Q.; Barber, A. H. Deformation and failure mechanisms in graphene oxide paper using in situ nanomechanical tensile testing. *Carbon* **2013**, *63* (0), 471−477.
(13) Espinosa, H. D.; Bernal, R. A.; Filleter, T. In Situ TEM Electromechanical Testing of Nanowires and Nanotubes. *Small* **2012**, *8* (21), 3233−3252.
(14) Espinosa, H. D.; Filleter, T.; Naraghi, M. Multiscale Experimental Mechanics of Hierarchical Carbon-Based Materials. *Adv. Mater.* **2012**, *24* (21), 2805−2823.
(15) Zhang, Y.; Liu, X.; Ru, C.; Zhang, Y. L.; Dong, L.; Sun, Y. Piezoresistivity Characterization of Synthetic Silicon Nanowires Using a MEMS Device. *J. Microelectromech. Syst.* **2011**, *20* (4), 959−967.
(16) Zhang, P.; Ma, L.; Fan, F.; Zeng, Z.; Peng, C.; Loya, P. E.; Liu, Z.; Gong, Y.; Zhang, J.; Zhang, X.; Ajayan, P. M.; Zhu, T.; Lou, J., Fracture toughness of graphene. *Nat. Commun.* **2014**, *5*, 10.1038/ncomms4782.
(17) Brown, J. J.; Suk, J. W.; Singh, G.; Baca, A. I.; Dikin, D. A.; Ruoff, R. S.; Bright, V. M. Microsystem for nanofiber electro-mechanical measurements. *Sens. Actuators, A* **2009**, *155* (1), 1−7.
(18) Zhao, J.; Pei, S.; Ren, W.; Gao, L.; Cheng, H.-M. Efficient Preparation of Large-Area Graphene Oxide Sheets for Transparent Conductive Films. *ACS Nano* **2010**, *4* (9), 5245−5252.
(19) Shojaei-Baghini, E.; Zheng, Y.; Sun, Y. Automated micropipette aspiration of single cells. *Ann. Biomed. Eng.* **2013**, *41* (6), 1208−16.
(20) Egerton, R. *Electron energy-loss spectroscopy in the electron microscope*; Springer Science & Business Media: New York, 2011.
(21) Suk, J. W.; Piner, R. D.; An, J.; Ruoff, R. S. Mechanical Properties of Monolayer Graphene Oxide. *ACS Nano* **2010**, *4* (11), 6557−6564.
(22) Lerf, A.; He, H.; Forster, M.; Klinowski, J. Structure of Graphite Oxide Revisited‖. *J. Phys. Chem. B* **1998**, *102* (23), 4477−4482.
(23) Chen, H.; Filleter, T. Effect of structure on the tribology of ultrathin graphene and graphene oxide films. *Nanotechnology* **2015**, *26* (13), 135702.
(24) Griffith, A. A. The Phenomena of Rupture and Flow in Solids. *Philos. Trans. R. Soc., A* **1921**, *221* (582-593), 163−198.
(25) Daly, M.; Reeve, M.; Veer Singh, C. Effects of topological point reconstructions on the fracture strength and deformation mechanisms of graphene. *Comput. Mater. Sci.* **2015**, *97*, 172−180.
(26) Zhou, S.; Bongiorno, A., Origin of the Chemical and Kinetic Stability of Graphene Oxide. *Sci. Rep.* **2013**, *3*, 10.1038/srep02484.
(27) Erickson, K.; Erni, R.; Lee, Z.; Alem, N.; Gannett, W.; Zettl, A. Determination of the Local Chemical Structure of Graphene Oxide and Reduced Graphene Oxide. *Adv. Mater.* **2010**, *22* (40), 4467−4472.
(28) Mkhoyan, K. A.; Contryman, A. W.; Silcox, J.; Stewart, D. A.; Eda, G.; Mattevi, C.; Miller, S.; Chhowalla, M. Atomic and Electronic Structure of Graphene-Oxide. *Nano Lett.* **2009**, *9* (3), 1058−1063.
(29) Compton, O. C.; Cranford, S. W.; Putz, K. W.; An, Z.; Brinson, L. C.; Buehler, M. J.; Nguyen, S. T. Tuning the Mechanical Properties of Graphene Oxide Paper and Its Associated Polymer Nanocomposites by Controlling Cooperative Intersheet Hydrogen Bonding. *ACS Nano* **2012**, *6* (3), 2008−2019.
(30) Medhekar, N. V.; Ramasubramaniam, A.; Ruoff, R. S.; Shenoy, V. B. Hydrogen Bond Networks in Graphene Oxide Composite Paper: Structure and Mechanical Properties. *ACS Nano* **2010**, *4* (4), 2300−2306.
(31) Shimizu, F.; Ogata, S.; Li, J. Theory of Shear Banding in Metallic Glasses and Molecular Dynamics Calculations. *Mater. Trans.* **2007**, *48* (11), 2923−2927.
(32) Freiman, S. W.; Mulville, D. R.; Mast, P. W. Crack propagation studies in brittle materials. *J. Mater. Sci.* **1973**, *8* (11), 1527−1533.
(33) Kim, S.; Zhou, S.; Hu, Y.; Acik, M.; Chabal, Y. J.; Berger, C.; de Heer, W.; Bongiorno, A.; Riedo, E. Room-temperature metastability of multilayer graphene oxide films. *Nat. Mater.* **2012**, *11* (6), 544−549.
(34) Weibull, W. A statistical distribution function of wide applicability. *J. Appl. Mech.* **1951**, *18*, 293−297.

DOI: 10.1021/acs.nanolett.5b02173
Nano Lett. 2015, 15, 6528−6534